Optimising the detection parameters for deep tissue photoacoustic imaging

T.J. Allen and P.C. Beard
Department of Medical Physics and Bioengineering, University College London,
Gower Street, London, WC1E6BT, UK

ABSTRACT

For deep tissue photoacoustic imaging, piezoelectric ultrasound detectors with large element sizes (>1mm) and relatively low centre frequencies (<5MHz) are generally used, as they can provide the required high sensitivity to achieve imaging depths of several centimetres. However, these detectors are generally not optimised in terms of element size and bandwidth. To identify these parameters in order to improve SNR and spatial resolution, two models were employed. The first was a numerical model and was used to investigate the effect of varying the detector element size on the amplitude and SNR of photoacoustic images. The second model was used to optimise the detector bandwidth. For this, the frequency content of simulated photoacoustic signals were studied for a range of depths and acoustic source sizes. The model was based on an analytical solution to the wave equation for a cylindrical source and incorporated the effects of frequency dependent acoustic attenuation. These models provide a new framework for optimising the design of photoacoustic scanners for breast and other deep tissue imaging applications.

Keywords: Photoacoustic imaging, Breast imaging,

1. INTRODUCTION

Photoacoustic imaging is a hybrid imaging technique which exploits the high contrast and specificity of optical imaging techniques and the high spatial resolution (<100μm) of ultrasound[1]. The technique is well suited to imaging the superficial (<1cm) microvasculature, due to the strong optical absorption of blood. Preclinical applications such as imaging the mouse brain[2], embryos[3], skin[4] and subcutaneous tumours[5] have been demonstrated. Imaging at greater depths (several cm) as required for applications such as breast imaging[6–8] represents a significant challenge due to the strong optical and acoustic attenuation of biological tissue. For example, for an effective attenuation coefficient of $1.3mm^{-1}$, as found in breast tissue[9], the optical penetration depth (the depth at which the fluence has decreased by 1/e) is approximately 8mm. For each additional centimetre of penetration depth, the fluence will therefore be attenuated by approximately a factor of 4. As a result the acoustic pressures generated at the source are relatively weak (tens of Pa) and are then further reduced by acoustic attenuation.

To achieve the large penetration depths (>5cm) necessary for deep tissue imaging, careful design of the detector element size and bandwidth is required. The aim of this study was to determine the optimum detector element size and bandwidth for deep tissue imaging application, using two models. The first, discussed in section 2, was implemented using a Matlab toolbox known as k-wave[10]. This toolbox was used to simulate the generation, propagation and detection of photoacoustic signals in a 2D cylindrical imaging geometry for different detector element sizes. The toolbox was also used to reconstruct photoacoustic images from the simulated signals using acoustic time reversal. The second model is discussed in section 3, and is based on an analytical solution to the wave equation for a cylindrical source and was used to investigate the effects of acoustic attenuation and source size on the bandwidth of the detected photoacoustic signals.

2. EFFECTS OF VARYING THE ELEMENT SIZE

To study the effect of varying the lateral dimension of the detector d, a 2D cylindrical scanning system was simulated using k-wave. k-wave[10] is a Matlab toolbox for modelling the propagation of acoustic waves through homogenous or heterogeneous media in one, two or three dimensions. The acoustic model is based on a pseudo-spectral time domain

Photons Plus Ultrasound: Imaging and Sensing 2012, edited by Alexander A. Oraevsky, Lihong V. Wang,
Proc. of SPIE Vol. 8223, 82230P · © 2012 SPIE · CCC code: 1605-7422/12/$18 · doi: 10.1117/12.908813

solution to the coupled first-order acoustic equations. To simulate a 2D cylindrical scanning system, the propagation of acoustic waves from an initial pressure distribution was modelled and recorded by a number of detectors evenly spaced along a circular scan line. The scanning radius was 4.5cm. The grid size was 1024×1024 pixels, each of dimensions 100μm×100μm and the maximum frequency supported by the model was 7.5MHz. The propagation medium was treated as homogenous and acoustically absorbing, for which the acoustic absorption coefficient followed a frequency power law of the form $\alpha = \alpha_0 f^y$ where α_0=*0.75dB/MHz/cm* and *y=1.5* for breast tissue[11]. The recorded acoustic waves were then used to reconstruct a photoacoustic image using a time reversal reconstruction algorithm also provided by the k-wave toolbox.

Two cases were studied. The first case, illustrated in Figure 1 (a), consists of a sparsely sampled scan in which the detectors were located at regular intervals along the scan line. The number of detectors was kept constant and only their lateral dimensions d were varied. This case is of interest as in practice it is often necessary to limit the number of detectors in order to avoid excessive cost and technical complexity. The second case illustrated in Figure 1 (b), consists of a fully sampled scan where the number of detectors is the maximum number that can be fitted around the scan line – ie the number of elements scales inversely with d. In both cases, the initial pressure distribution was composed of five point sources labelled P1 to P5. P1 is located at the centre of scan whereas P2, P3, P4 and P5 are located at distances of 8, 16, 24 and 32mm from the centre of the circular scan line, respectively. The amplitudes corresponding to the acoustic point sources in the reconstructed photoacoustic images were recorded as d was varied.

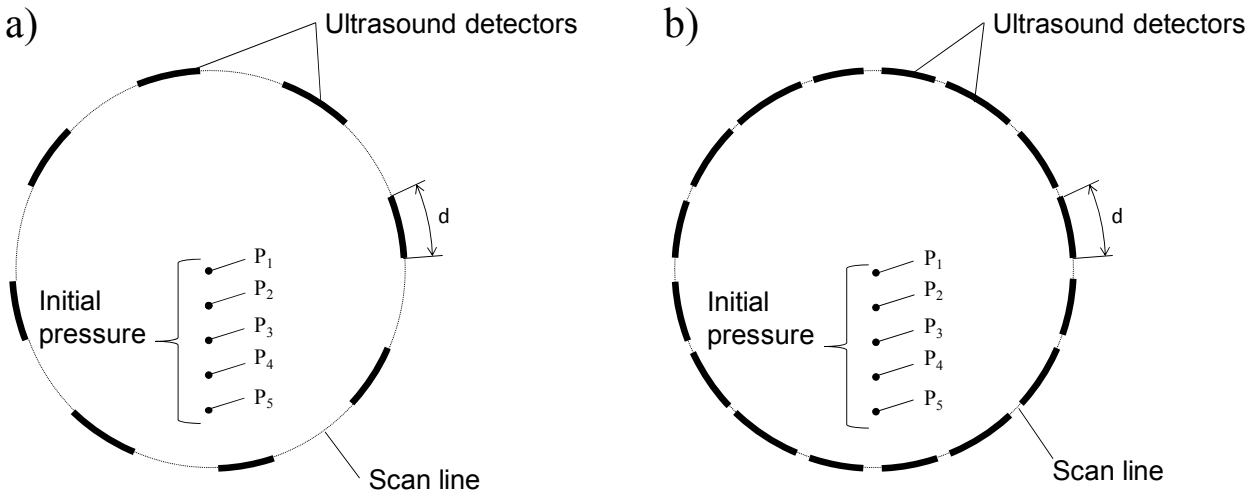

Figure 1: Schematic of the initial pressure distribution and detector configuration. d is the lateral dimension of the detectors. (a) sparsely sampled and (b) fully sampled scan. The initial pressure distributions are composed of 5 acoustic point sources labelled P1 to P5. P1 is located at the centre of scan whereas P2, P3, P4 and P5 are located at 8, 16, 24, and 32mm from the centre of scan, respectively.

Figure 2 (a) shows the results obtained for the sparsely sampled scan. As d increases, the amplitudes of the reconstructed point sources get larger. These changes in amplitude are a consequence of the sensitivity of the detector increasing as d increases. The increase in the amplitudes of P2 to P5 with increasing d, gradually flattens out. This is because the detectors become increasingly more directional thus exhibiting lower sensitivity to acoustic waves at oblique angles. By contrast, the acoustic waves generated at P1 located at the centre of scan, will be normally incident on all detectors and so the amplitude increases linearly with d.

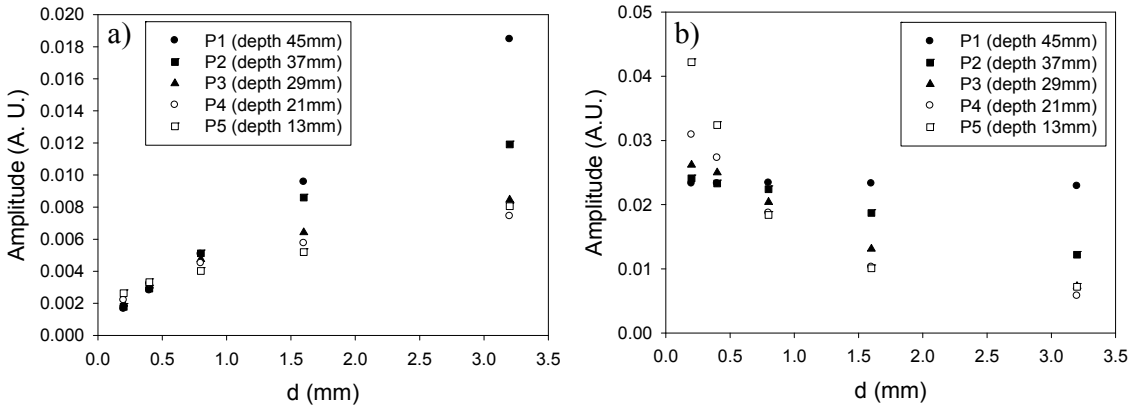

Figure 2: Effects of increasing d on the amplitude of the point sources P1 to P5 in the reconstructed photoacoustic image for (a) sparsely and (b) fully sampled scan

Figure 2 (b) shows the results obtained for the fully sampled scan. As d increases, the amplitude of the reconstructed acoustic sources decreases, except for P1 where the amplitude remained constant. For the fully sampled scan the number of detectors used decreases with increasing d and therefore no increase in amplitude is observed unlike the partial scan case.

In order to investigate the effects of varying d on the SNR and spatial resolution of the photoacoustic images, an initial pressure distribution composed of five acoustic sources of 0.3mm in diameter (labelled A' to E' in figure 3 (a)) and five acoustic sources of 0.5mm in diameter (labelled A to E in figure 3 (a)) was modelled. The initial pressure of these acoustic sources were set to 33Pa, corresponding to the pressure generated by a source with an absorption coefficient of $10mm^{-1}$ embedded at a depth of 5cm in a medium with an effective attenuation coefficient of $1.3mm^{-1}$ and an incident fluence of $20mJ/cm^2$. Noise was added to the detected photoacoustic signals so that the noise equivalent pressure of a 0.2mm detector was 2.5Pa. Figure 3 (b) shows a photoacoustic image obtained when using 45 detectors and d=0.2mm. This configuration corresponds to a sparsely sampled scan. Due to the relatively low pressure reaching the detectors (as low as 0.15Pa), the smaller acoustic sources, labelled A' to E' in figure 3 (a), are barely visible in the reconstructed image.

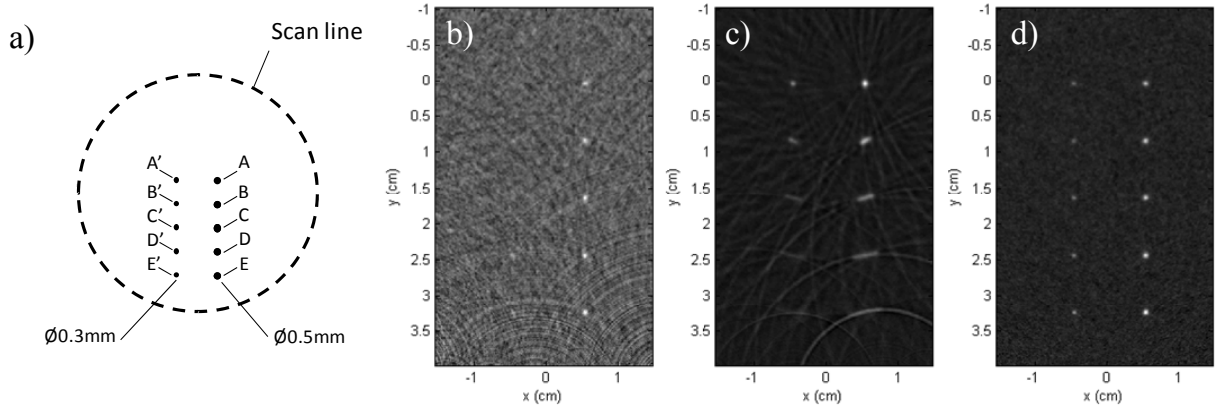

Figure 3: (a) Schematic of the initial pressure distribution and the detector scan line. Reconstructed photoacoustic images using (b) N=45, d=0.2mm (c) N=45, d=4.8mm (d) N=1080, d=0.2mm where N is the number of detectors used and d the lateral dimension of the detectors.

Figure 2 (a) suggests that in the sparse scan configuration, if the total number of detectors used is limited (45 in this example) the amplitude of the acoustic sources in the reconstructed images can be increased by increasing d. To illustrate the effect of increasing d, figure 3 (c) shows a reconstructed photoacoustic image obtained when using 45 detectors of 4.8mm diameter. The improvement in the SNR of the image is noticeable with A' and B' now visible in figure 3 (c). However, the acoustic sources located further away from the centre of scan, for example those labelled D and E in figure 3 (a), are now difficult to identify.

When operating in a fully sampled scan configuration, figure 2 (b) suggests that reducing d in order to reduce the directionality of the detector will result in an increase in the amplitude of the reconstructed features. To illustrate this point, figure 3 (d) shows a photoacoustic image obtained when using 1080 detectors and d=0.2mm. Each individual acoustic source is visible in the reconstructed photoacoustic image and no obvious degradation in lateral resolution was observed. The FWHM of the acoustic source corresponding to the source labelled E in figure 3 (a) was measured to be 0.5mm, in agreement with the true value of 0.5mm.

For an additional comparison of all three imaging configurations, a profile through the larger acoustic sources (A to E) was obtained (at x=0.5mm) for each reconstructed image and is showed in figure 4. As suggested by the results in figure 2, when d is large (e.g. 4.8mm), the amplitude of the reconstructed acoustic sources located further away from the centre of scan are significantly lower than those located close to the centre of scan. For example, in figure 4 the amplitude corresponding to source A is 0.4 whereas the amplitude corresponding to source E is 0.14. Once again this is due to increased directionality of the detector with increasing d. For the smaller (0.2mm) less directional detectors the amplitude remains relatively constant for each acoustic source.

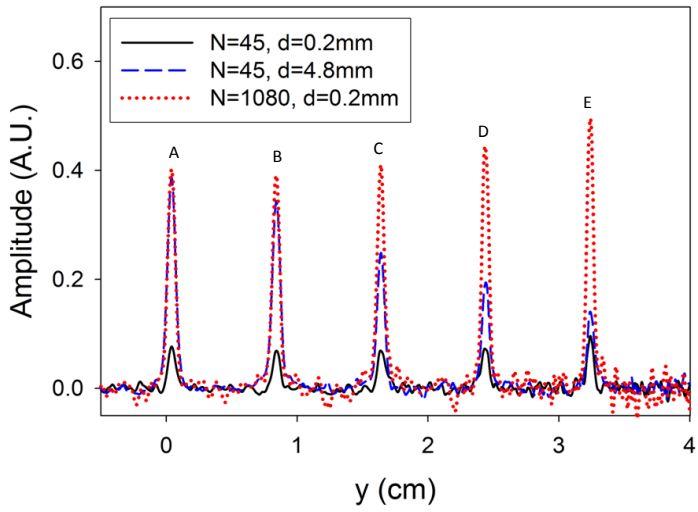

Figure 4: Profiles obtained at x=0.5cm through the reconstructed photoacoustic images shown in figure 3 (b-d), where N is the number of detectors used and d the lateral dimension of the detector.

To compare the performances of the different imaging configurations, the SNRs corresponding to the acoustic sources (A to E) are showed in table 1. For the sources located away from the centre of the scan (B, C, D and E), the small element size detectors (0.2mm) outperform the larger detectors (4.8mm) in a fully sampled scan. However, for the acoustic source A, the larger detectors provided higher SNR than the 0.2mm detectors. Figure 4 shows that the amplitude obtained at point A for both detectors is relatively similar (approximately 0.4); it is the background noise which has changed. This is because the noise scales as a function of $\sqrt{N}$ where N is the total number of detector used. Also the presence of artefacts in the image will increase as the number of detectors used for the reconstruction is reduced and d increases.

	N=45, d=0.2mm	N=45, d=4.8mm	N=1080, d=0.2mm
Source A	9.3	35	26.4
Source B	8.9	22.5	27.9
Source C	11.2	13.8	28.4
Source D	10.6	11.5	30.9
Source E	13.1	10.7	36.3

Table 1: SNR obtained from the reconstructed photoacoustic images shown in figure 3 (b-d), measured for each of the 0.5mm acoustic sources labelled A to E in figure 3 (a). N is the number of detectors used and d the lateral dimension of the detector.

3. OPTIMISING THE DETECTOR BANDWIDTH

To determine the optimum detector bandwidth it is necessary to determine the frequency content of the photoacoustic signals reaching the tissue surface. An analytical solution[12] to the wave equation was therefore used to simulate a pressure wave *p(t)* generated by a cylindrical source after propagating a distance z. This analytical solution assumes that the absorbed optical density is uniformly distributed throughout the cylindrical source. The photoacoustic signals were then Fourier transformed to obtain their spectral content and the effect of frequency dependent acoustic attenuation *A(f)* was then incorporated as follows

$$P_d(t) = IFFT[FFT(p(t) \times A(f)] \qquad \textbf{(1)}$$

where

$$A(f) = \mathrm{e}^{-\alpha z} \qquad \textbf{(2)}$$

and α is the acoustic absorption coefficient expressed as $\alpha = \alpha_0 f^y$ (For breast tissue α_0=*0.75dB/MHz/cm* and *y=1.5*) [11].

Figure 5 (a) shows an example of a photoacoustic signal generated in a 100μm diameter cylindrical source at a depth of 5cm. The acoustic attenuation coefficient was set to α_0=*0.75dB/MHz/cm* and *y=1.5* which corresponds to the values of breast tissue[11]. Figure 5 (b) shows the spectrum of the same photoacoustic signal. The minimum (f_{min}) and maximum (f_{max}) detectable frequencies were defined as the lowest and largest frequency components for which their amplitudes were 40dB smaller than the peak amplitude of the spectrum, as illustrated in figure 5 (b).

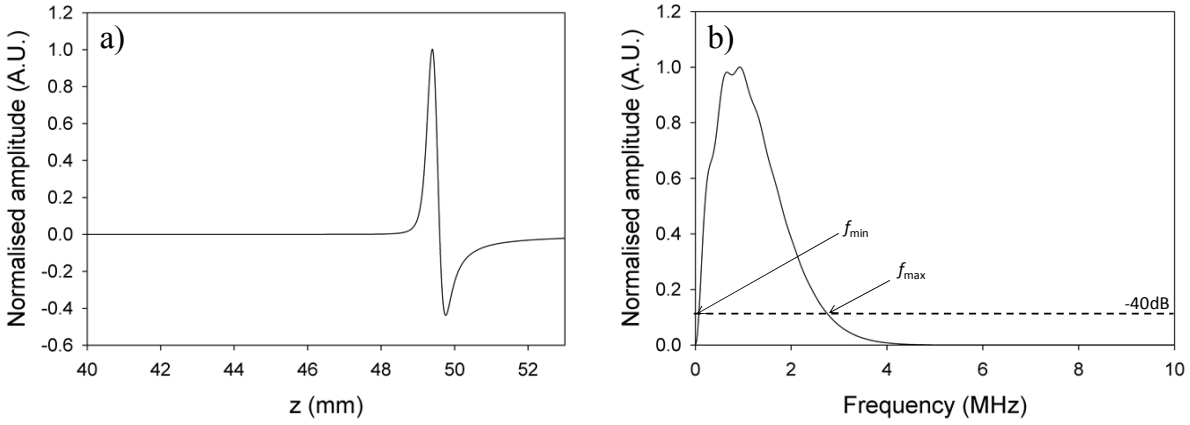

Figure 5: Photoacoustic signal generated in a 100μm diameter cylindrical source at a depth of 5cm. The acoustic attenuation coefficient was set to *α_0=0.75dB/MHz/cm* and *y=1.5*. (a) Time domain signal and (b) frequency spectrum

Photoacoustic signals generated for a range of depths (1cm to 5cm) and source sizes (10 to 500μm) were then simulated in order to determine the optimum bandwidth for deep tissue photoacoustic imaging. Figure 6 shows the minimum and maximum detectable frequencies of the simulated photoacoustic signals as a function of depth and source size. The high frequency components of the photoacoustic signals have been strongly attenuated by the frequency dependent acoustic attenuation of tissue. For example, for a 10μm diameter source the maximum detectable frequency is approximately 4MHz for a penetration depths in excess of 5cm whereas for a penetration depths of 1cm the maximum detectable frequency is about 10MHz. Figure 6 also shows that the minimum detectable frequency decreases with increasing depth, suggesting that ultrasound detectors which are able to detect frequencies down to a few hundred KHz are required for deep tissue photoacoustic imaging. The minimum detectable frequency for a depth of 5cm is approximately 0.22MHz.

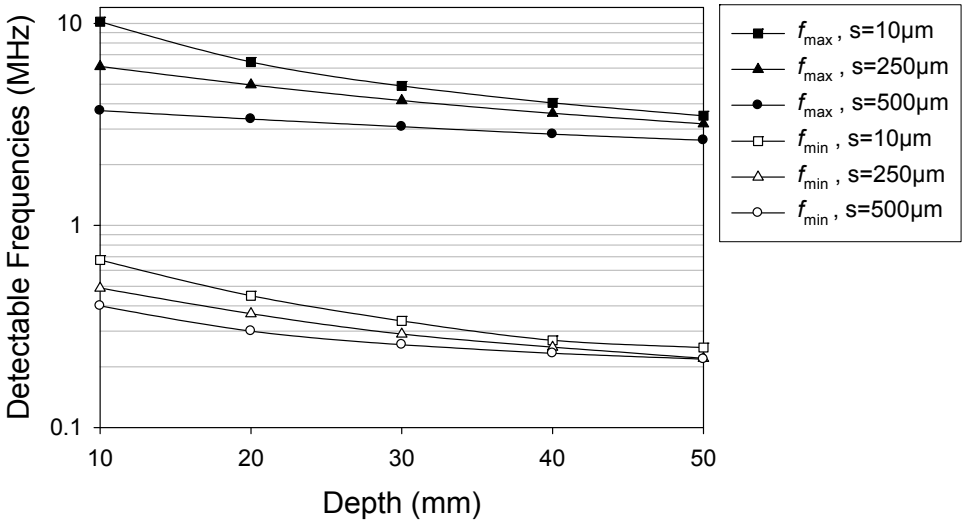

Figure 6: Minimum (f_{min}) and Maximum (f_{max}) detectable frequency as a function of depth. The photoacoustic signals were generated in cylindrical sources for a range of depths and sizes (where s is the diameter of the cylindrical source). The acoustic attenuation coefficient was set to $\alpha_0=0.75dB/MHz/cm$ and $y=1.5$.

4. DISCUSSION

Although figure 3 (d) suggests that for a fully sampled scan, the use of omnidirectional detectors would maximise the amplitude of the reconstructed acoustic sources, it was shown that this did not always result in the SNR being maximised. For example the SNR of the reconstructed acoustic source A was smaller when d=0.2mm than for d=4.8mm (see table 1). This is because the noise floor in the reconstructed image increases as a function of the square root of the number of detectors. The use of the smaller detectors (d=0.2mm) however had the advantage of providing higher SNRs for the reconstructed acoustic sources located further away from the centre of scan (e.g. sources B, C, D and E). They also provided higher lateral resolution and reduced artefacts in the reconstructed photoacoustic image.

It was also shown that, as the response of the detectors becomes increasingly directional, further increasing d only improves the SNR for acoustic sources located close to the centre of scan, whereas the SNR of sources located further away from the centre of scan decreases. For photoacoustic imaging of the breast it is important to maximise the SNR for acoustic sources located deep within the tissue (close to the centre of scan) as the acoustic pressures generated by these sources will be weak. If this is achieved by increasing element size this will inevitably compromise the SNR yielded by superficial sources.

5. CONCLUSION

This study has provided guidelines for optimising the element size of the ultrasound detectors used in a cylindrical scanning system. It was shown that to maximise the sensitivity of the imaging system at depth it may be necessary to compromise the lateral resolution and SNR of sources located close to the tissue surface. The analytical model showed that ultrasound detectors which are able to detect frequencies as low as a few hundreds of KHz to up to 4MHz are required for penetration depths >5cm. The models developed in this study provide a new framework for optimising the design of photoacoustic scanners for breast and other deep tissue imaging applications.

REFERENCES

1. Beard, P. Biomedical photoacoustic imaging. *Interface Focus* **1**, 602-631 (2011).

2. Laufer, J., Zhang, E., Raivich, G. & Beard, P. Three-dimensional noninvasive imaging of the vasculature in the mouse brain using a high resolution photoacoustic scanner. *Applied Optics* **48**, D299-306 (2009).

3. Laufer, J., Cleary, J., Zhang, E., Lythgoe, M. & Beard, P. Photoacoustic imaging of transgenic mouse embryos. *Biomedical Optics* paper BWE7 (2010).

4. Zhang, E.Z., Laufer, J.G., Pedley, R.B. & Beard, P.C. In vivo high-resolution 3D photoacoustic imaging of superficial vascular anatomy. *Physics in Medicine and Biology* **54**, 1035-46 (2009).

5. Laufer, J. *et al.* In vivo longitudinal photoacoustic imaging of subcutaneous tumours in mice. *Proceedings of SPIE* **7899**, 789915-1-789915-6 (2011).

6. Kruger, R.A., Lam, R.B., Reinecke, D.R., Del Rio, S.P. & Doyle, R.P. Photoacoustic angiography of the breast. *Medical Physics* **37**, 6096 (2010).

7. Piras, D., Steenbergen, W., van Leeuwen, T.G. & Manohar, S.G. Photoacoustic Imaging of the Breast Using the Twente Photoacoustic Mammoscope: Present Status and Future Perspectives. *IEEE Journal of Selected Topics in Quantum Electronics* **16**, 730-739 (2010).

8. Ku, G. & Wang, L.V. Deeply penetrating photoacoustic tomography in biological tissues enhanced with an optical contrast agent. *Optics Letters* **30**, 507-9 (2005).

9. Durduran, T. *et al.* Bulk optical properties of healthy female breast tissue. *Physics in Medicine and Biology* **47**, 2847-61 (2002).

10. Treeby, B.E. & Cox, B.T. k-Wave: MATLAB toolbox for the simulation and reconstruction of photoacoustic wave fields. *Journal of Biomedical Optics* **15**, 021314 (2010).

11. Szabo, T.L. *Diagnostic Ultrasound Imaging*. (Elsevier Academic Press: London, 2004).

12. Diebold, G.J. & Sun, T. Properties of Photoacoustic Waves in One, Two and Three Dimensions. *Acustica* **80**, 339-351 (1994).